REPORT DOCUMENTATION PAGE

1. REPORT DATE (DD-MM-YYYY) February 2013	2. REPORT TYPE Technical Paper	3. DATES COVERED (From - To) February 2013-May 2013
4. TITLE AND SUBTITLE X-ray Radiography Measurements of Shear Coaxial Rocket Injectors		**5a. CONTRACT NUMBER** In-House
		5b. GRANT NUMBER
		5c. PROGRAM ELEMENT NUMBER
6. AUTHOR(S) S. A. Schumaker, M. Lightfoot, S.A. Danczyk, R.N. Bernstein, and A.L. Kastengren		**5d. PROJECT NUMBER**
		5e. TASK NUMBER
		5f. WORK UNIT NUMBER Q0X3
7. PERFORMING ORGANIZATION NAME(S) AND ADDRESS(ES) Air Force Research Laboratory (AFMC) AFRL/RQRC 10 E. Saturn Blvd. Edwards AFB CA 93524-7680		**8. PERFORMING ORGANIZATION REPORT NO.**
9. SPONSORING / MONITORING AGENCY NAME(S) AND ADDRESS(ES) Air Force Research Laboratory (AFMC) AFRL/RQR 5 Pollux Drive Edwards AFB CA 93524-7048		**10. SPONSOR/MONITOR'S ACRONYM(S)**
		11. SPONSOR/MONITOR'S REPORT NUMBER(S) **AFRL-RQ-ED-TP-2013-037**

12. DISTRIBUTION / AVAILABILITY STATEMENT

Distribution A: Approved for Public Release; Distribution Unlimited. PA#13169

13. SUPPLEMENTARY NOTES

Conference paper for the 25th Annual ILASS-Americas Conference, Pittsburgh, PA, 5-8 May 2013.

14. ABSTRACT

Shear coaxial injectors are a common injector type for liquid-rocket-propulsion applications and can be found in many oxygen/hydrogen engines. These injectors rely on the shear between an outer lower-density, high-velocity annulus and a higher-density, low-velocity inner jet to atomize and mix the propellants. Because of the dense-jet core, the optical densities of these sprays are high, particularly near the injector where primary atomization and flame holding take place. The large optical density has prevented interrogation, detailed study, and understanding of this important region. The evolution of x-ray radiography techniques using intense x-ray sources (such as Argonne National Laboratory's Advanced Photon Source) has allowed the measurement of quantitative equivalent path lengths and projected densities in the near-injector regions of shear coaxial injectors. Using water and gaseous nitro-gen as propellant simulants at atmospheric backpressure, the effect of momentum flux ratio and mass flux ratio, are investigated for three injector geometries operating at momentum flux ratios spanning the range from 0.5 to 15.

15. SUBJECT TERMS

16. SECURITY CLASSIFICATION OF:			17. LIMITATION OF ABSTRACT	18. NUMBER OF PAGES	19a. NAME OF RESPONSIBLE PERSON Stephen Schumaker
a. REPORT Unclassified	**b. ABSTRACT** Unclassified	**c. THIS PAGE** Unclassified	SAR	15	**19b. TELEPHONE NO** (include area code) 661-525-5165

X-Ray Radiography Measurements of Shear Coaxial Rocket Injectors

S. A. Schumaker[*], M.D.A. Lightfoot, S.A. Danczyk and R. N. Bernstein
Air Force Research Laboratory
Edwards AFB, CA 93524 USA

A.L Kastengren
Argonne National Laboratory
Argonne, IL 60439 USA

Abstract

Shear coaxial injectors are a common injector type for liquid-rocket-propulsion applications and can be found in many oxygen/hydrogen engines. These injectors rely on the shear between an outer lower-density, high-velocity annulus and a higher-density, low-velocity inner jet to atomize and mix the propellants. Because of the dense-jet core, the optical densities of these sprays are high, particularly near the injector where primary atomization and flame holding take place. The large optical density has prevented interrogation, detailed study, and understanding of this important region. The evolution of x-ray radiography techniques using intense x-ray sources (such as Argonne National Laboratory's Advanced Photon Source) has allowed the measurement of quantitative equivalent path lengths and projected densities in the near-injector regions of shear coaxial injectors. Using water and gaseous nitrogen as propellant simulants at atmospheric backpressure, the effect of momentum flux ratio and mass flux ratio, are investigated for three injector geometries operating at momentum flux ratios spanning the range from 0.5 to 15.

---

[*]Corresponding author: Stephen.Schumaker@edwards.af.mil

Introduction

Due to their utility in a number of combustion devices (turbofan engine exhaust, air blast furnaces, and liquid rocket engines) shear coaxial jets have been studied for over sixty years [1]. In all applications the complex near field (two annular shear layers in close proximity) is of critical importance in determining system performance. In rocket engines, shear coaxial jets have been used as injectors for both boost class engines (SSME, Ariane 5) [2,3] and upper stage engines (J-2) [4]. Shear coaxial jets work well with propellant combinations and engine cycles that produce significant shear at reasonable pressure drops, such as H_2/LOX or CH_4/LOX engines using a fuel regeneratively cooled combustion chamber.

Previous coaxial jet research can be divided by the phase of the two fluids as either single or multiple phases. Most of the fundamental coaxial jet research has been done using a single phase (either gas-gas or liquid-liquid mixing). A brief review of single-phase coaxial jet research can be found in Schumaker and Driscoll [5]. Single-phase cases also include work where both fluids are supercritical, which is common in modern boost-class liquid rocket engines. Studies have indicated that "liquid" core coaxial jets operating at supercritical conditions scale in a similar-manner to single-phase coaxial jets. However, details and scaling constants differ [6].

The second class of coaxial jets operate with two different fluid phases. The gaseous high speed outer jet (fuel) is used to fragment a dense liquid core (oxidizer). This fluid configuration is common in upper-stage engines and during throttled conditions, startup and shutdown transients of boost-class engines. The current work focuses on this multiphase type of jet. Previous studies on two-phase coaxial jets have been more limited then single-phase work but not insubstantial. An excellent review on coaxial jet atomization can be found in an article by Lasheras and Hopfinger [7]. In these previous studies, optical imaging techniques have been used to study the liquid core breakup process and measure global spray structures such as liquid core length and spray angles [8, 9]. On the spray periphery and in the fair-field PDPA has been used to measure droplet sizes and velocities [9]. From these measurements regime diagrams have been developed along with scaling laws for the liquid core length and empirical correlations for spray angles and droplet distributions in the far-field [7, 9, 10]. The current study looks to add current understanding of the primary atomization region to the field by making the first quantitative measurements of mass density in near-field of shear coaxial jets.

In the past the exploration of the near-field region of dense sprays, such as the current coaxial jets, has been hampered by the elastic scattering that dominates visible light measurement techniques or perturbation of the flow field through intrusive measurements. X-ray radiography overcomes both of these issues, since the dominate interaction of photons in the x-ray part of the spectrum with droplets is absorption. Beer's law can be used to solve for a path integrated liquid-phase thickness or projected density, which provides a quantitative measure of the mass density at any location in the spray. Integrating a cross-sectional profile of the spray and dividing by the liquid-mass-flow rate allows a mass averaged velocity to be calculated.

In the recent years x-ray radiography has shown its usefulness by successfully interrogating the near field of a number of dense sprays including diesel injectors, aerated liquid jets, solid-cone sprays, impinging-jet sprays and gas-centered swirl-coaxial injectors [11-15]. While x-ray radiography can be performed using a synchrotron source or a tube source, a synchrotron source has a number of well-documented advantages over a tube source, notably possessing sufficient flux to produce a monochromatic beam [16]. The one large disadvantage of a synchrotron source is that the experiment must be brought to a synchrotron facility, and these facilities lack spray infrastructure. The issues of spray infrastructure have been largely overcome by the development of a mobile test rig that can deliver high flow rates and pressures of gaseous nitrogen and water while integrated into the 7-BM beamline of the Advanced Photon Source (APS) located at Argonne National Laboratory.

The present study uses x-ray radiography to measure centerline and radial profiles of Equivalent Path Length (EPL) in shear coaxial jet injectors. These profiles are used to investigate the effect of momentum flux ratio, mass flux ratio and post thickness on the liquid mass distribution in these sprays. Measurements span from the injector exit to the far-field. Centerline EPL profiles are used to define four atomization regions in the spray.

Experimental Methods

X-ray radiography measurements were performed at the 7-BM beamline at the Advanced Photon Source. The x-ray source for the beamline is a synchrotron bending magnet. This source produces polychromatic, nearly collimated radiation. A double-multilayer monochromator is used to produce a monochromatic ($\Delta E/E=1.4\%$) x-ray beam. Details regarding the beamline setup are given in Ref. [17]. For the current experiment a beam photon energy of 10 keV was used. Using a pair of Kirkpatrick-Baez focusing mirrors housed in the experimental enclosure the beam was focused to 7 μm vertical x 8 μm horizontal (full width at half maximum) at a flux of 1.6×10^{10} photons per second before the experimental apparatus. A silicon PIN diode was used as the detector. The photocurrent from this PIN

diode was amplified and time averaged over a 5 second integration time. One-dimensional transverse scans were made across the spray, perpendicular to the injector axis with a 0.25 mm step size. One-dimensional scans were also made on the spray centerline, parallel to the injector axis with a 0.25 mm step size. Radial scan widths varied between 8 and 16 mm depending on test condition and downstream location. Centerline scan were conducted between 0.25 and 25 mm downstream. For every flow condition transverse scans were performed 0.02, 0.5, 1, 2.5, 5, 10, 15 and 25 mm downstream of the injector face. No injector rotations were performed due to the high level of symmetry in the radial profiles.

The recorded signal level was converted to the Equivalent Path Length (EPL) of water using Beer's law

$$EPL = \frac{-\ln(I/I_0)}{\beta\rho}, \qquad (1)$$

where I is the intensity of the transmitted light, I_0 is the intensity of incident light, β is the mass attenuation coefficient, and ρ is the density of the absorbing fluid. Normalization by I_o was performed in two steps. First, each point in the scan was normalized by a corresponding beam intensity measured from an intensity monitor based on fluorescence from a thin titanium foil placed inline with the beam upstream of the spray. The I_o measurement accounts for changes in beam intensity during a scan. The second normalization baselines the intensity to the zero absorption case and uses the average signal level from the 5 points in the scan with the highest transmissions. These were points that are outside of the spray. Since centerline profiles (i.e. those parallel to the spray axis) contained no points outside of the spray, the centerline profiles were normalized using the same baselines as the 10 mm downstream radial (i.e. cross axis) profile.

The mass attenuation coefficient can be calculated using the NIST photon cross section database [18]; for pure water and a beam energy of 10 keV β=5.33 cm^2/g. Gas phase absorption is much less than the liquid phase absorption, therefore, only the liquid phase mass is measured. The EPL is the pathlength-integral of the amount of water in the beam. Interpretation of the EPL is discussed further in the Results and Discussion section. It should be noted that the use of monochromatic x-rays greatly simplifies the conversion of x-ray transmission to EPL; this is a significant advantage of synchrotron sources over laboratory x-ray sources.

Surrogate propellants (water and gaseous nitrogen) were delivered to the injector using a facility dubbed the Mobile Flow Laboratory (MFL). The MFL was designed to allow aerospace-propulsion injector testing at remote diagnostic facilities such as the APS that do not have the infrastructure to provide relevant flow conditions. The MFL is a self-contained system with its own data acquisition and control systems, allowing it to be run remotely. Liquid nitrogen, electrical power and an exhaust system are all that is required of the host facility. Gaseous nitrogen is produced from the liquid supply and is stored in two, 57-liter gas bottles. The gaseous nitrogen is also used to pressurize a 57-liter water tank. Gas and liquid flow rates are controlled using electronic pressure regulators with calibrated critical flow orifices. The system has an uncertainly of 4% in the gas flow rate and 1% in the liquid flow rate [19].

Three shear-coaxial jet injectors were used in the current study. These injectors are scaled up versions of injectors previously used by AFRL to study supercritical and acoustic effects on shear coaxial jets [20,21]. A schematic of the injector geometry is shown as Fig. 1 and a photo of the injector assembly is shown as Fig. 2. Table 1 lists critical injector dimensions. Due to space constraints in the test hutch, injectors were run in a horizontal orientation.

Test matrix

Flow conditions for each test case are provided in Table 2. For each injector geometry five nominal momentum flux ratio (Φ, defined as gas-to-liquid) conditions were run (Φ=0.5, 2, 5, 10, 15). Flow velocities were set so that the gas-jet Mach number was always less than 0.7.

Critical Parameters

Previous studies have shown that two-phase coaxial jets stability and atomization is controlled by six non-dimensional parameters [7]. These parameters are the liquid and gas Reynolds number (Re), the Ohnesorge number (Oh), the Weber number (We), the momentum flux ratio (Φ), and the mass flux ratio (m). Full definitions are provided in the nomenclature. In the current study the main parameters of interest are Φ and m. The mass flux ratio is defined liquid to gas. The values of Re_g, Re_l, Oh, and We are in a range that all conditions are within the fiber-type atomization regime identified by Lasheras and Hopfinger [7]. Since all flow conditions investigated here are in the same atomization regime and Re_g, Re_l, Oh, and We vary minimally, changes in these parameters are expected to have a negligible effect on the observable differences between test conditions. In the jet near-field, the shear, or nondimensionally the momentum flux ratio, between the two fluids controls primary atomization. The mass flux ratio plays a minimal role in the primary atomization region, but does affect secondary atomization and spray velocities by setting the relative amount of momentum that can be transferred from the gas to the liquid phase. At small

enough values, the mass flux ratio will play a role in the primary atomization region. It should be noted that injector area ratio effects are accounted for in m. For injectors SC4 and SC24 the post and inner jet geometry is the same, only the gas jet diameters differ. The same jet velocities were used for the matching momentum flux ratio test condition; therefore, a difference in the mass flux ratio is due solely to changes in the area ratio.

One geometric variable that is not accounted for in these six nondimensional parameters is the post thickness T_p. The post thickness' primary effect is to set the size of the post-tip recirculation zone which, indirectly, sets the boundary conditions for the interaction between the two fluid streams.

Results and Discussion

In this section experimental cases will be identified by the injector geometry, which sets important parameters like the area ratio and lip thickness, and the momentum flux ratio (Φ). Injector dimensions can be found in Table 1 and test condition parameters can be found in Table 2.

Figure 3 shows radial and centerline EPL profiles for injector SC4 operating at the five Φ values (0.5, 2, 5, 10 & 15). Close to the jet exit the EPL profiles have an elliptical shape due to the curvature of the liquid core- this shape is expected and has previously been seen in diesel injector studies [12]. Farther downstream the spray widens and the total EPL drops as the potential core is atomized and the droplets are accelerated by the higher-velocity outer-gas stream. It should be noted that EPL is a function of both the mass flux and velocity for droplet-laden flows [15]. So, while the EPL drops at farther downstream locations is partially due to jet spreading, the more significant factor causing decreases in EPL is the acceleration of the droplets to higher velocities. In the current work liquid exit velocities are between 2-6 m/s while gas exit velocities vary between 87-230 m/s (Table 2).

One of the strengths of the x-ray technique is the ability to make quantitative measurements extremely close to the injector face. In the present study the nearest measurements were made 0.02 mm downstream of the injector face. The minimum measurement distance from the face is set by the ability of the researcher to eliminate wetting of the injector face and the angular alignment of the injector to the beam. Note that the zero location was set as the point where the injector cut the X-ray beam, decreasing the intensity on the pin diode by half. The importance of making measurements close to the injector exit is evident in Figs. 3a & f, where for the Φ=0.5 case the liquid core diameter is seen to contract at the jet exit and then expand at 2.5 mm downstream before decreasing again. This contraction and dilation also occurs at Φ=0.5 with the other two injector

geometries (Figs. 4a & 5a). The quantitative data also show a steep drop-off in EPL. For example, with for geometry SC4 operating at Φ=15, the EPL has already decreased by 13% at 0.5 mm downstream (L/D$_l$=0.2) versus at the injector exit (0.02 mm). Clearly, critical information can be lost if measurements cannot be made at the injector outlet.

In almost all cases (Figs. 3, 4, 5) the peak EPL value differs (both high and low) from the liquid jet diameter; 2.08, 2.79 and 2.79 mm for injectors SC1, SC4 and SC24, respectively. For most cases this difference is small (<6%), but for other cases it can be quite substantial (>60%). With the exception of Φ=0.5 conditions always having a contraction and then a dilation, no clear trend with momentum flux is observed that explains the small variations in peak EPL from the jet diameter. Four possibilities exist for these variations: atomization, surface waves, peak EPL not resolved, and water in the post recirculation. Except at high Φ (>10), meaningful atomization is unlikely in the near-injector region (here, taken as 0.02-0.5 mm downstream), so EPL rates smaller than the jet diameter are unexpected. Surface waves are unlikely to alter average liquid core thicknesses, since the long integration time used in the current study (5 seconds) allows for averaging across many cycles. One likely cause of the observed dilation is the peak value is simply being missed due to the radial step size (0.25 mm). EPL values higher than the liquid exit diameter can be attributed to water in the tip recirculation zone. The shoulders on the 0.02 mm downstream EPL profiles in Figs. 5a, b, c, d, & e (SC1) are evidence of water in the tip recirculation zones. The large lip in SC1 creates a substantial recirculation zone, so significant H$_2$O entrainment is expected. These possibilities will be explored in the future using high speed microscopic imaging of the near injector region.

The effect of the momentum flux ratio on the dark core length of two-phase coaxial jets is well documented in previous studies and a number of scaling laws for the dark core length have been derived with Φ as the primary scaling parameter [7]. Centerline EPL profiles (Figs. 3f, 4f, 5f) show the same general trend reported in these studies, increasing Φ increases primary atomization, thus shortening the liquid core. The shortening of the liquid core with increasing Φ can be seen in the centerline EPL profiles by observing the slope decrease from the near-injector region towards the far-field and the transition region (bend in the EPL).

Figure 6 shows centerline EPL profiles normalized by the liquid inlet diameter and plotted against a normalized downstream distance (X/D_l) allowing geometries with different liquid jet diameters to be compared. From these and other dimensional EPL profiles (Figs. 3f, 4f & 5f) four unique atomization regions can be identified. The first region is the near-injector that is

4

characterized by either a constant or slight increase in the centerline EPL immediately following the injector exit. The shape of this near-injector region and/or its existence is governed by Φ, the injector post geometry, and jet exit velocity profiles. In the case of the thick lip configuration (SC1) this region can extend up to 3 X/D_l (Fig. 6a). This length is not universal across varying injector post geometries, however. The near-injector region exists due to boundary conditions created by the post geometry that delays interaction of the two streams. The two largest drivers are the post recirculation zone and the velocity boundary layers at the jet exits.

The second region is the primary atomization region or core breakup region which is characterized by a nearly linear decline in EPL. The slope of this section is related to the atomization rate and, therefore, controlled by Φ. This core breakup region should be nearly independent of the area ratio except for very small values. The post thickness and, therefore, the size of the recirculation zones can also play a role, as is evident in Fig. 5f for the SC1 geometry which has the thick post. After delaying atomization it is unclear if this change is due to increased atomization, thinning of the recirculation zone, or downstream acceleration of the droplets in the recirculation zone. Unfortunately the x-ray radiography technique cannot distinguish between liquid in the jet, spray, or recirculation zone.

The third region is the transition between core breakup and the far-field. The transition region is characterized by a clear change of slope in the centerline profiles. As Φ increases the angle of change of derivative is lessened and the length of the region decreases. The fourth and final region is the far-field zone. Secondary atomization is of primary importance. EPL continues to decrease as the spray widens, droplets break apart and accelerate to higher velocities. This region again has a nearly linear slope. Here, though, the slope is set by both Φ and m. The lower the mass flux ratio, for a given momentum flux ratio, the greater the relative amount of momentum the gas can transfer to the liquid resulting in faster, smaller droplets which produces a lower EPL value.

In the past studies these four regions have been largely defined based on semi-quantitative backlit imaging techniques where light intensity levels have been used to judge the core break up length and overall structure [6, 9]. Droplet size and velocity measurements have been limited to well within the far field or only on the very periphery of the spray [9]. Since EPL can be formulated in terms of a quantitative projected density these types of measurements can be used to further characterize these regions and refine scaling constants in atomization models. This work is, regrettably, left to the future. Additionally time-resolved x-ray measure-

ments may be able to shine light on the surface wave structures, droplet size and velocities in all regions.

An additional parameter of importance in coaxial jet atomization is the mass flux ratio (defined liquid-to-gas). Injectors SC4 (Fig. 3) and SC24 (Fig. 2) have the same liquid jet geometry (T_p & D_l) but different area ratios, 11.46 and 3.4, respectively. The same jet velocities were used for the matching momentum flux ratio test condition; therefore, a difference in the mass flux ratio for injector SC4 and SC24 is due solely to changes in the area ratio. This change in area ratio results in a 3.4 times increase in m for injector SC24 compared to injector SC4 under the same injection conditions (velocities and densities). Decreasing m results in more gas jet momentum (relative to total jet momentum) being available to transfer to the liquid jet. Increased momentum transfer leads to faster atomization and higher droplet velocities in the far-field region. Higher droplet velocities result in lower EPL values.

The effect of mass flux ratio is clearest when plotting the normalized centerline EPL profiles from all three geometries at the same Φ value on a single plot (Figure 6). It is immediately clear that the SC1 geometry is an outlier from the other two geometries due to the large recirculation zones that form behind the thick injector post. These recirculation zones and their effect on the EPL make it impossible to compare SC1 directly with the other two geometries. However; SC1 has a similar mass flux ratios to SC4 (0.71 compared to 0.81 for $\Phi=10$), so it is expected that differences between SC1 and SC4 are largely the result of the recirculation zones on the atomization and not mass flux ratio effect.

As expected, injectors SC4 and SC24 are very similar in the core breakup region indicating that m has little impact on primary atomization. Small differences in this region are likely due to the small differences in Φ (Table 2) between the two injectors. In the transition and the far-field regions for $\Phi= 0.5$ & 2.0 (Figs. 6a & b) the EPL for the lower m value injector (SC4) drops below the higher m value injector (SC24) indicting faster momentum transfer in the far-field region at low m and, therefore, resulting in smaller and faster droplets as m decreases. An unexpected result is that at $\Phi= 15$ (Fig. 6c) no difference is seen in the EPL profiles between the two injectors. The collapse of these two EPL profiles indicates that conditions can be reached where momentum transfer between the gas and the liquid is no longer limited by the total momentum available and droplet velocity and size has plateaued.

It should be noted that when the centerline profiles for injector geometries SC4 and SC24 (Figs. 3f & 4f) are compared at the $\Phi=5$ and 10 test conditions, significant variations are observed in the near-injector region. It is believed that this variation is due to a normalization issue with these centerline profiles. Since the cen-

terline profiles contain no zero absorption points out of the spray, centerline profiles were normalized by the baseline observed in the 10 mm downstream radial profiles (roughly the half-way point of the centerline profiles) at the same flow conditions. A more complex normalization scheme is likely required to account for varying levels of background mist at different axial locations.

X-ray radiography can also be used to measure the mass-weighted velocity of the liquid phase at downstream locations. The mass-weighted velocity (U_{ma}) is obtained by dividing the liquid mass flow rate with the integral of the average liquid density profile [22]. This integral measures all liquid mass in the 2D cross-section perpendicular to the injector axis is counted. Figure 7 shows mass-weighted velocities for all test conditions. The two thinner lip injectors have mass averaged velocities at the jet exit that agree well with liquid jet exit velocities calculated from the experimentally metered mass flow rates (Table 2). Due to the significant amount of liquid mass trapped in the post recirculation zones, U_{ma} at the jet exit for the thicker lip post (Fig. 7c) are well below the calculated liquid jet velocities. The effect m can have on the spray in the far-field is evident when U_{ma}, is compared between injectors SC4 and SC24 (same lip thickness) for Φ=10. This large decrease in m is sufficient to raise U_{ma} from 23.3 m/s to 44.6 m/s. This change in average droplet velocity demonstrates the significant effect the relative momentum between the two jets can have on the droplets in the far-field.

Summary and Conclusions

X-ray radiography was used to quantitatively examine shear coaxial jet injectors. This work is the first time quantitative measurements of the mass density have been obtained in the near-injector region of this injector type. Radial profiles of EPL were made as close as 0.02 mm from the injector exit. The effects of momentum flux ratio and mass flux ratio were explored for three injector geometries. EPL profiles taken on the injector centerline show the same general trend reported in studies of the dark core length, increasing momentum flux ratio increases primary atomization thus shortening the liquid core. Mass flux ratio was shown to have a minimal impact on the primary atomization zone but can alter the droplet velocities in the far-field by limiting the relative amount of momentum the gas jet can transfer to the liquid phase. Centerline profiles were used to define four spray regions: near-injector, primary atomization, transition, and far-field. In the future these quantitative measurements of projected density and mass averaged velocity will be used to further characterize these regions and refine scaling constants in atomization models.

Nomenclature

A	jet area
D	jet diameter
I	intensity of transmitted light
I_o	intensity of incident light
L	jet inlet length
m	mass flux ratio, $\rho_l U_l A_l / \rho_g U_g A_g$
$\dot{m}$	mass flow rate
Oh	Ohnesorge number, $\mu_l/(\rho_l \sigma_l D_l)^{1/2}$
Re_g	gas Reynolds number, $U_g(D_g\text{-}(D_l+2T_p))/\nu_g$
Re_l	liquid Reynolds number, $U_l D_l / \nu_l$
r	radial coordinate
x	downstream coordinate
T	thickness
U	velocity
We	Weber number, $\rho_g U_g^2 D_l/\sigma$
Φ	momentum flux ratio, $\rho_g U_g^2 / \rho_l U_l^2$
β	mass attenuation coefficient
ρ	density
σ	surface tension
ν	kinematic viscosity
μ	viscosity

Subscripts

g	gas
l	liquid
ma	mass averaged
p	injector post

References

1. Forstall, W., and Shapiro, A.H., *Journal of Applied Mechanics* 18:399-408 (1950).
2. Sutton, G.P., and Biblarz, O., *Rocket Propulsion Elements: An Introduction to the Engineering of Rockets*, Wiley-Interscience, 2001.
3. Juniper, M., Tripathi, A., Scouflaire, P., Rolon, J.-C., and Candel, S., *Sixth International Conference on Liquid Atomization and Spray Systems*, Edinburgh, Scotland, July 2000, pp. 1103-1109.

4. Hulka, J. and Hutt, J.J., *Liquid Rocket Engine Combustion Instability*, Edited by Yang, V. and Anderson, W., AIAA, 1995.

5. Schumaker, S.A., and Driscoll, J.F., *Physics of Fluids* 24: 055101 (2010).

6. Davis, D.W., Chehroudi, B., and Talley, D.G., *10th International Congress on Liquid Atomization and Spray Systems*, Kyoto, Japan, Aug. 2006.

7. Lasheras, J.C., and Hopfinger, E.J., *Annual Review of Fluid Mechanics* 32:275-308 (2000)

8. Davis, D.W., and Chehroudi, B., *Journal of Propulsion and Power* 23:364-374 (2007).

9. Lasheras, J.C., Villermaux, E., and Hopfinger, E. J., *Journal of Fluid Mechanics* 357:351-379 (1998).

10. Rehab, H., Villermaux, E., and Hopfinger, E. J., *Journal of Fluid Mechanics* 345:357-381 (1997).

11. Leick, P., Kastengren, A.L., Liu, Z., Wang, J., and Powell, C.F., *11th Triennial International Conference on Liquid Atomization and Spray Systems*, Vail, Colorado, July 2009.

12. Kastengren, A. L., Powell, C. F., Liu, Z., Moon, S., Gao, J., Zhang, X., and Wang, J., *22nd Annual Conference on Liquid Atomization and Spray Systems*, Cincinnati, Ohio, May 2010.

13. Lin, K.C., Carter, C., Smith, S., and Kastengren, A., *50th AIAA Aerospace Sciences Meeting*, Nashville, Tennessee, January 2012.

14. Halls, B. R., Heindel, T.J., Meyer, T.R., and Kastengren, A.L., *50th AIAA Aerospace Sciences Meeting*, Nashville, Tennessee, January 2012.

15. Schumaker, S.A., Kastengren, A.L., Lightfoot, M.D.A., Danczyk, S.A., and Powell, C.F., *12th International Conference on Liquid Atomization and Spray Systems*, Heidelberg, Germany, September 2012

16. Heindel, T. J., *Journal of Fluids Engineering*, 133-7, (2011).

17. Kastengren, A.L., Powell, C. F., Arms, D., Dufresne, E. M., Gibson, H. and Wang, J., *Journal of Synchrotron Radiation* 19:654-657 (2012).

18. Berger, M.J., Hubbell, J.H., Seltzer, S.M., Chang, J., Coursey J.S., Sukumar, R., Zucker, D.S., and Olsen, K., *XCOM: Photon Cross Sections Database, NIST Standard Reference Database 8 (XGAM)*, http://www.nist.gov/pml/data/xcom/index.cfm.

19. Lightfoot, M.D.A., Schumaker, S.A., Villasmil, L.A., and Danczyk, S.A., *JANNAF 8th Modeling and Simulation, 6th Liquid Propulsion, and 5th Spacecraft Propulsion Joint Subcommittee Meeting*, Huntsville, Alabama, December 2011, http://handle.dtic.mil/100.2/ADA554873.

20. Teshome, S., Leyva, I.A., Rodriquez, J., and Talley, D., *12th International Conference on Liquid Atomization and Spray Systems*, Heidelberg, Germany, September 2012.

21. Teshome, S., Leyva, I.A., Talley, D., and Karagozian, A.R. *50th AIAA Aerospace Sciences Meeting*, Nashville, Tennessee, January 2012.

22. Kastengren, A., Powell, C.F., Wang, Y.-J, IM, K.-S., and Wang, J., *Atomization and Sprays*, 19, 1031-1044 (2009).

Figure 1. Injector schematic: (a) cross-sectional view, (b) Injector SC1, (c) Injector SC4, (d) Injector SC24
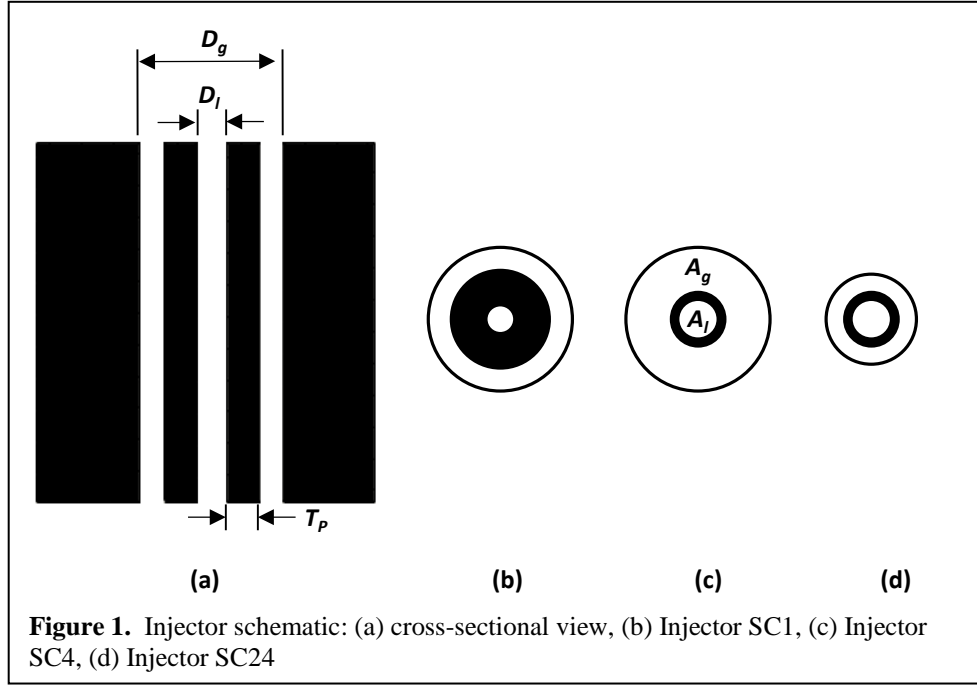
Table 1. Injector dimensions.

Injector	D_l (mm)	D_g (mm)	T_p (mm)	L_l/D_l	A_g/A_l
SC1	2.08	10.2	2.32	48.8	13.4
SC4	2.79	10.2	0.457	36.4	11.5
SC24	2.79	6.35	0.457	36.4	3.40

**Table 2.** Test conditions with mass flow rates and relevant nondimensional parameters.

| Condition	Φ	U_g (m/s)	U_l (m/s)	$\dot{m}_g$ (g/s)	$\dot{m}_l$ (g/s)	m	We	Re_g	Re_l
SC1-0.5	0.50	87	4.0	2.20	13.6	3.25	395	9,060	8,250
SC1-2	2.0	170	4.0	4.20	13.6	1.60	1580	19,100	8,250
SC1-5	5.0	231	3.5	4.20	11.9	0.99	3030	28,500	7,220
SC1-10	10	189	2.0	4.30	6.80	0.71	1980	21,500	4,120
SC1-15	15	229	2.0	4.20	6.80	0.57	2960	27,400	4,120
SC4-0.5	0.50	129	6.0	9.80	36.7	3.76	689	25,600	16,600
SC4-2	2.0	230	5.5	18.5	33.6	1.82	2320	48,900	19,600
SC4-5	5.0	231	3.5	18.6	21.4	1.15	2340	49,800	12,500
SC4-10	10	233	2.5	18.8	15.3	0.81	2390	51,500	8,930
SC4-15	15	229	2.0	18.4	12.2	0.66	2300	51,500	7,140
SC24-0.5	0.50	129	6.0	2.90	36.7	12.7	689	10,500	16,600
SC24-2	2.0	230	5.5	5.50	33.6	6.13	2320	20,000	16,600
SC24-5	5.0	231	3.5	5.50	21.4	3.87	2340	20,400	15,500
SC24-10	10	233	2.5	5.60	15.3	2.74	2390	21,100	8,930
SC24-15	15	229	2.0	5.50	12.2	2.24	2300	21,100	7,140

**Figure 2.** Photo of injector assembly.
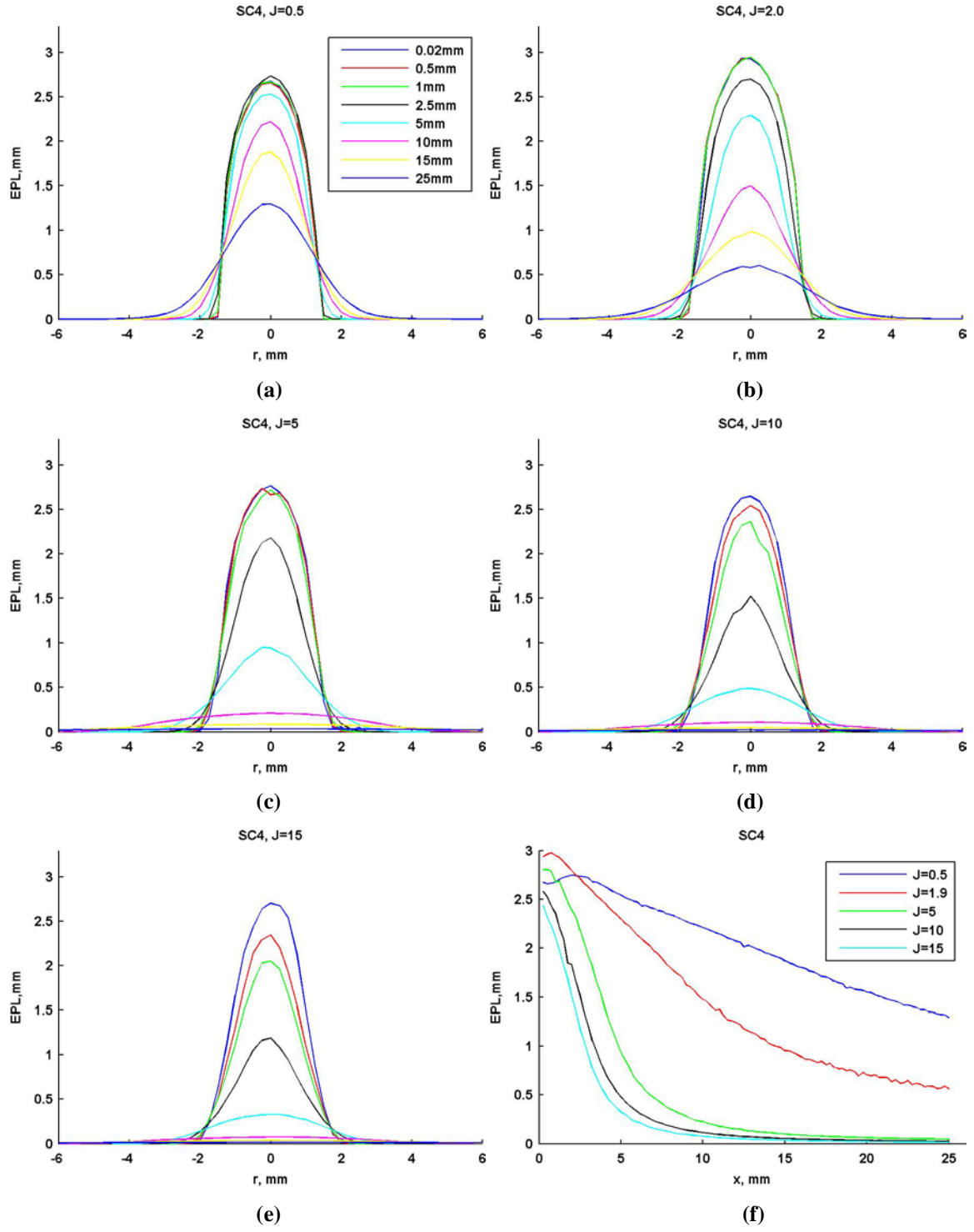
Figure 3. Radial EPL profiles for injector SC4 at Φ values of (a) 0.50, (b) 2.0, (c) 5.0, (d) 10, and (e) 15. (f) Centerline EPL profiles for injector SC4.
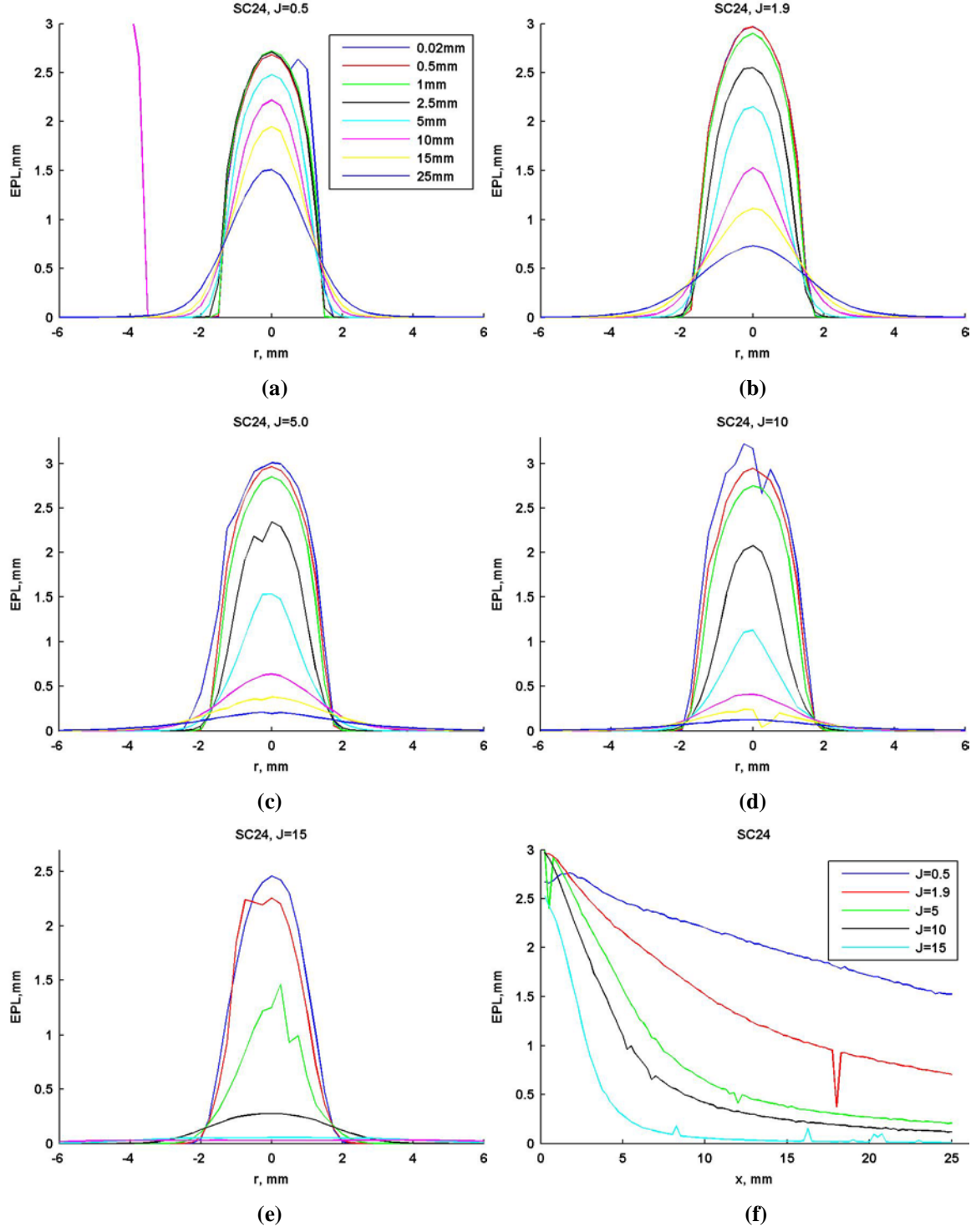
Figure 4. Radial EPL profiles for injector SC24 at Φ values of (a) 0.50, (b) 2.0, (c) 5.0, (d) 10, and (e) 15. (f) Centerline EPL profiles for injector SC4.
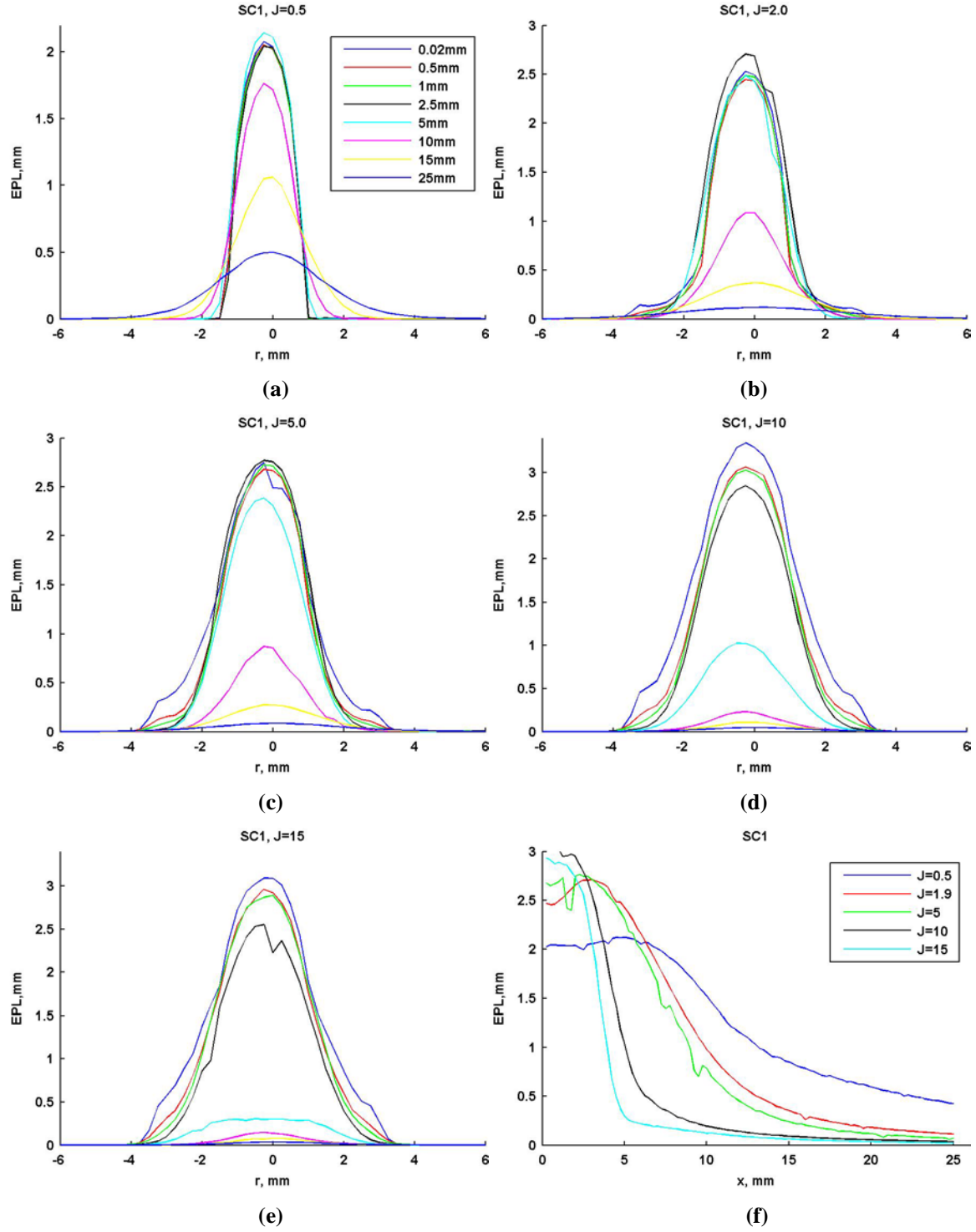
Figure 5. Radial EPL profiles for injector SC1 at Φ values of (a) 0.50, (b) 2.0, (c) 5.0, (d) 10, and (e) 15. (f) Centerline EPL profiles for injector SC4.
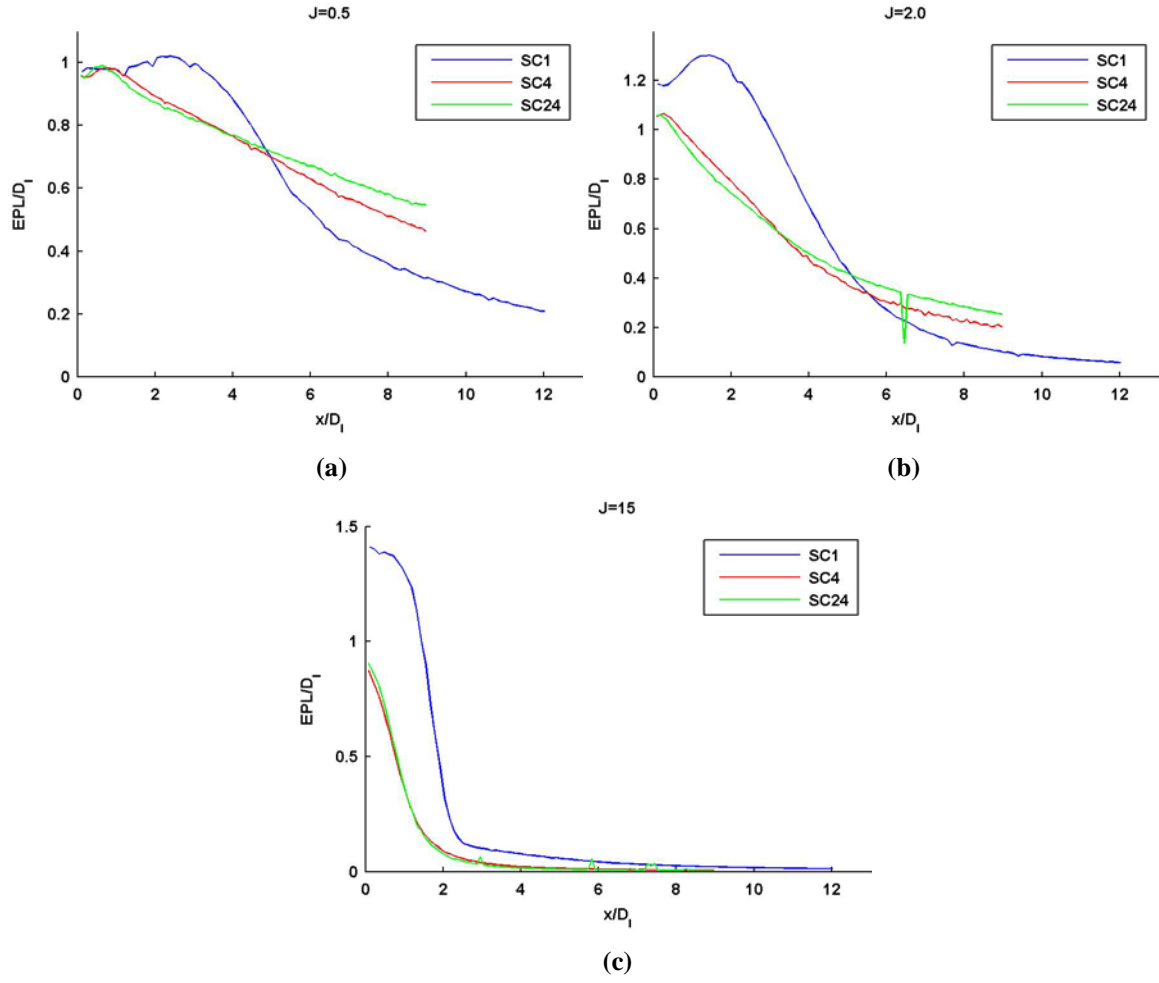
Figure 6. Centerline EPL profiles for injectors SC1, SC4, and SC24 normalized by Dl for nominal Φ values of (a) 0.5, (b) 2.0, and (c) 15.
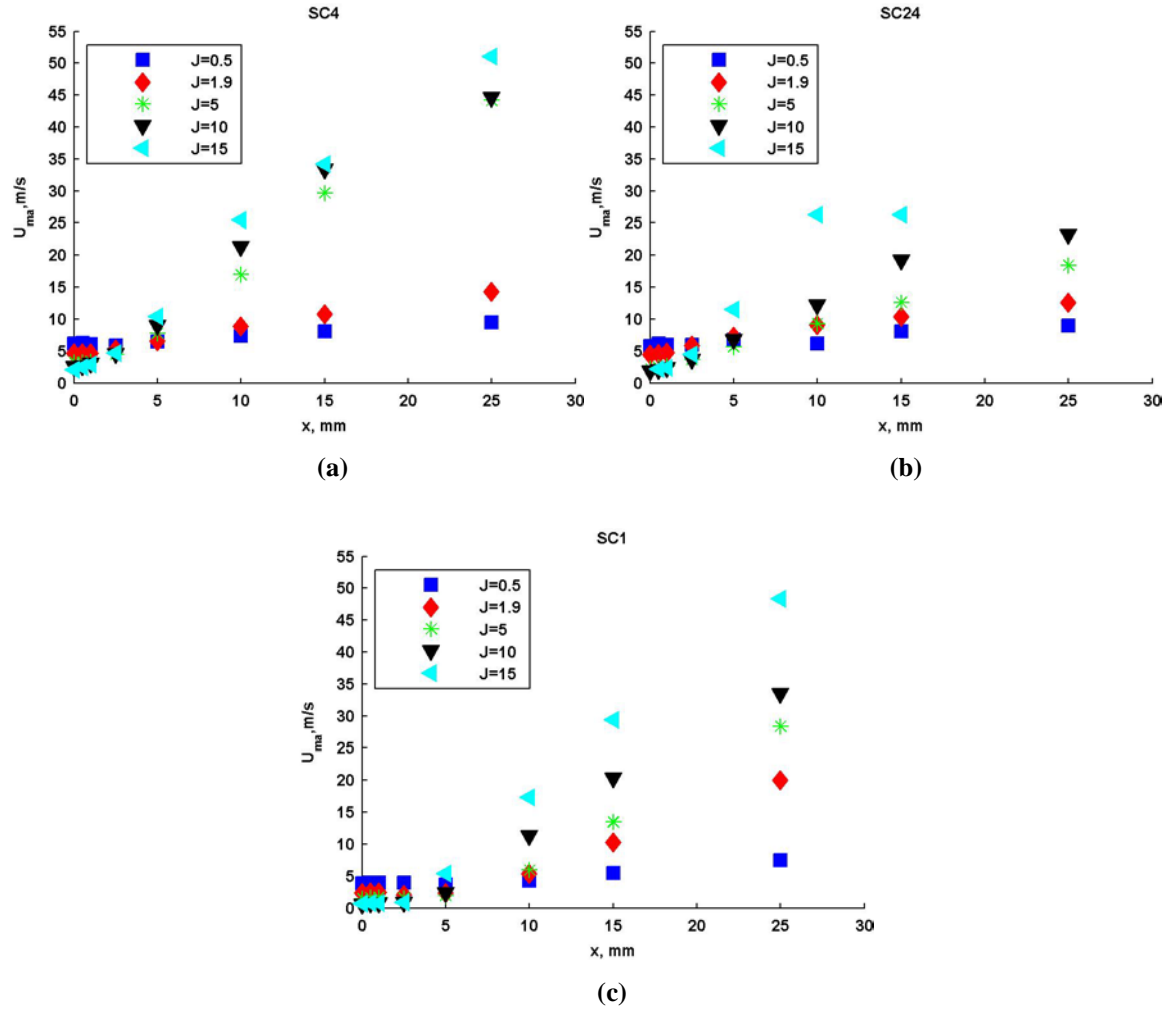
Figure 7. Plots of mass averaged velocity (U_{ma}) for injectors (a) SC4, (b) SC24, and (c) SC1.